EEG-guided Robotic Mirror Therapy System for Lower Limb Rehabilitation

Yeganeh M. Marghi[1], Amir B. Farjadian[2], Sheng-Che Yen[3], Deniz Erdogmus[1]

Abstract— **Lower extremity function recovery is one of the most important goals in stroke rehabilitation. Many paradigms and technologies have been introduced for the lower limb rehabilitation over the past decades, but their outcomes indicate a need to develop a complementary approach. One attempt to accomplish a better functional recovery is to combine bottom-up and top-down approaches by means of brain-computer interfaces (BCIs). In this study, a BCI-controlled robotic mirror therapy system is proposed for lower limb recovery following stroke. An experimental paradigm including four states is introduced to combine robotic training (bottom-up) and mirror therapy (top-down) approaches. A BCI system is presented to classify the electroencephalography (EEG) evidence. In addition, a probabilistic model is presented to assist patients in transition across the experiment states based on their intent. To demonstrate the feasibility of the system, both offline and online analyses are performed for five healthy subjects. The experiment results show a promising performance for the system, with average accuracy of 94% in offline and 75% in online sessions.**

I. Introduction

Functional recovery following stroke is largely dependent on neuroplasticity [1]. To induce neuroplasticity and drive motor recovery, rehabilitation interventions should focus on inducing concurrent activation of sensory feedback loops and sensorimotor motor cortex to restore corticospinal connections. Most existing rehabilitation programs use bottom-up approaches to induce neuroplasticity [2]. In this approach, intervention is done on the peripheral limb aiming to elicit neuroplasticity in the central nervous system (CNS). One example is body weight support treadmill training (BWSTT) where patients practice stepping on a treadmill in an intensive manner while a human therapist or a robot attempts to move and adjust their leg into a predetermined normal one. This approach generates ascending proprioceptive feedback that is consistent with a normal gait, which is thought to be a driving force for neuroplasticity. However, the effectiveness of BWSTT is suboptimal, and whether the peripheral intervention affects CNS remains unclear [3].

Another predominant rehabilitation approach to induce neuroplasticity is the top-down approach [2]. In this approach, the intervention is directly applied to the CNS aiming to elicit functional improvement in the peripheral limb. Mirror therapy is one of the most studied top-down approaches that has shown positive effects on functional recovery [4]. During this therapy, a mirror is used to reflect the motion of the unaffected limb. The mirror image is then superimposed on the unmoving affected limb. Studies have shown that observing the mirror image can activate the hemisphere controlling the affected limb [5] and in turn improve its function. Since the affected limb is not moving during the therapy, proprioceptive feedback plays a minimal role in driving neuroplasticity.

To accomplish a better functional recovery, researchers have tried to combine the bottom-up and top-down approaches by means of brain-computer interface (BCI) [6], [7]. BCIs by recording, decoding, and translating measurable brain signals into an effector action or behavior, are potentially a powerful tool for being part of the rehabilitation. One of the most popular neurophysiological phenomena used in BCI research is the modulation of sensorimotor rhythms through motor imagery [8], [9]. Imagination of a limb movement produces a distinctive pattern on the motor cortex that can be detected in real-time from the EEG signal. Imagination of a movement, engages the primary motor cortex in a comparable way to how motor execution does. There are several reports of EEG-based system for rehabilitation in stroke patients, but the majority of these reports for stroke recovery focus on the rehabilitation of upper limbs [7], specifically of hand movements.

In this study, an EEG-guided robotic mirror therapy system is proposed for lower limb rehabilitation. We present a paradigm to combine robotic training (bottom-up) and mirror therapy (top-down) approaches. This paradigm includes four states to synchronize the two approaches and assist patients in lower limb rehabilitation according to their intention. To achieve the synchronization, a BCI system is implemented, which classifies the EEG evidence by extracting features from collected data. The EEG evidence feeds a probabilistic model using a finite-state Markov chain to assist patients in transition across states.

II. Methods

Fig. 1 illustrates the proposed EEG-guided robotic system for lower limb rehabilitation. The system consists of the following components: (i) a mirror placed in between legs, which reflects the image of the non-affected leg movement; (ii) a wearable accelerometer to measure ankle range of motion of the non-affected leg; (iii) the virtually-interfaced

*This research is supported by NSF (IIS-1149570, CNS-1544895), NIDLRR (90RE5017-02-01), NIH (R01DC009834), and Northeastern University TIER 1 Award.

[1]Yeganeh M Marghi and Deniz Erdogmus are with the Cognitive Systems laboratory (CSL), Electrical and Computer Engineering Department, Northeastern University, Boston, MA, USA (corresponding authors e-mail:ymmarghi@ece.neu.edu)

[2]Amir B. Farjadian is with the Department of Mechanical Engineering, Massachusetts Institute of Technology (MIT), Cambridge, MA, USA.

[3]Sheng-Che Yen is with the Department of Physical Therapy, Movement and Rehabilitation Science, Northeastern University, Boston, MA, USA.

978-1-5090-2809-2/17/$31.00 ©2017 IEEE

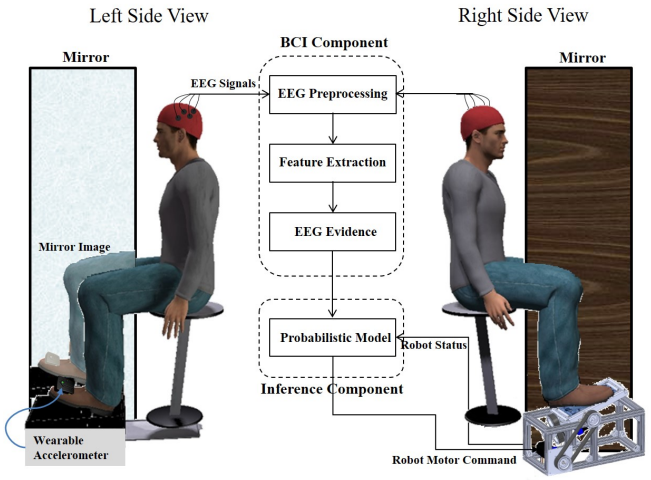

Fig. 1. Representation of the EEG-guided robotic mirror therapy system for lower limb rehabilitation. The picture illustrates the setup from both sides of the mirror.

Robotic Ankle and Balance Trainer (vi-RABT) [10] that assists the ankle motion in the affected side; (iv) a BCI component that infers the patient's intent by classifying the measured and processed EEG; (v) an inference component that is a probabilistic model for the inter-state transitions between different experiment states according to the EEG evidence and robot status (e.g. on/off). The system is designed such that the mirror reflects the movement of the unaffected limb to form an illusory limb, which is visually superimposed on the affected limb. By observing the illusory limb movement and imagining that this is the movement performed by the affected limb, the neurons in the sensorimotor cortex of the injured hemisphere can be activated [8]. The neural activities are captured and analyzed by the BCI component. The detected EEG evidence and current status of the robot are integrated in the inference component to assist the subject to move the affected ankle.

A. Robotic Instrumentation

vi-RABT [10] is a 2-DOF robotic footplate that can be effectively used in physical therapy of ankle deficits, balance disorders and variety of mobility impairments, such as stroke. vi-RABT is equipped with two gear-motors, which provide actuated assistive therapy along dorsiflexion/plantarflexion (DFPF) and inversion/eversion (INEV) axes of the ankle joint and the power from both gear-motors is transmitted by a pulley timing belt to the robotic footplate. The angular displacement along each axis is measured by an optical encoder installed in the closest proximity to the footplate. In the current setup, the robot is using the angle of the non-affected ankle (NAFA) to move the affected ankle (AFA) along the DFPF axes. For that purpose, DELSYS® Trigno™ wireless systems with accelerometer sensors is used to measure the angle of NAFA. The sampling rate and measurement range of the accelerometer sensor are 148.1 Hz and $\pm$6g, respectively.

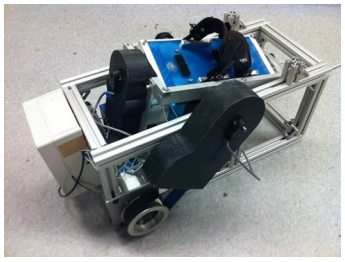

Fig. 2. The virtually-interfaced robotic ankle and balance trainer (vi-RABT) that is a robotic footplate with 2-DOF actuation.

B. Experiment Paradigm

The experiment consists of two sessions, i.e. calibration (offline) and online sessions. The calibration session is used for training the BCI component. The online session includes the proposed therapy method. Each session consists of four states, i.e. $\{\mathbf{s}_k\}_{k=0}^{3}$. In all states, subjects are asked to move the NAFA, keep it in dorsiflexion for six seconds, and then relax by following an audio trigger. Each set of measured EEG after receiving the auditory stimulus is considered one trial. The dorsiflexion ankle movement is defined as **Go** trial. In state $\mathbf{s}_0$, the subject is looking to a fixed point on the wall and the robot is off and does not move the AFA. In $\mathbf{s}_1$, the subject is looking in the mirror and is perceiving the mirror image as the movement of the AFA, but the robot is off. $\mathbf{s}_2$ is same as $\mathbf{s}_1$, except that the robot is on and is moving the AFA. $\mathbf{s}_3$ also is the same as $\mathbf{s}_0$, except that the robot is on and is moving the AFA.

During the calibration session, subjects are asked to complete 60 trials for each state. They are also offered to have a 5-minute break before starting the next state. It should be noted that the calibration session does not have particular order and can be performed in any combination of states. During the online session, the process always starts from state $\mathbf{s}_0$, which means the robot is off and the subject is asked to move their NAFA without looking at the mirror. Whenever the subject is ready for the mirror imagination part, she/he looks at the mirror and tries to imagine the mirror image as the movement of the AFA. By inducing imagination, the neurons in the sensorimotor cortex of the injured hemisphere get activated. According to the detected EEG evidenced in BCI component that is the probabilist measure of the patient intent, inference component will activate the robot to assist the subject in moving the AFA. The robot will keep moving the affected limb, as long as the subject can focus on the mirror image. Whenever the subject gets tired (mentally/physically) the robot will be stopped by the inference component. During the online session, the BCI and inference components are using the last observed EEG evidence for every single **Go** trial.

C. BCI Component

EEG data is collected using g.tec g.USBamp EEG amplifiers (Guger Technologies OG). An active set of EEG electrodes derived by an AC g.Gammabox is used in all the experiments. EEG signals are collected from C2, C4, C6, and CP4 channels in case of injury on the right hemisphere, and

C1, C3, C5, and CP3 channels in case of injury on the left. The EEG was sampled at 256 Hz with 60 Hz notch filter. The reference and ground electrodes are located on right ear lobe and nasion, respectively. As a preprocessing step, the EEG signal is filtered with an FIR band-pass filter in 0.5-30 Hz band, which includes frequency components of the EEG related to movement actions and imagination. The signals are down sampled to 64 Hz. First two seconds of all trials have been excluded to avoid movement artifacts affecting the data analysis. At each trial, the data $\mathbf{E}_i \in \mathbb{R}^{d \times n_{st}}$ from all channels is windowed to 500 ms segments, then concatenated such that $d = ch \times m$, where ch, m, and n_{st} are number of channels, number of samples in each time window, and number of subtrial in i-th trial, respectively.

In BCI applications, extracting EEG features that provide the most information about the intention of the user is one of the main challenges. One method suggested for this purpose, particularly regarding imaginations and movement actions, is the Common Spatial Pattern (CSP) [11]. It has since become popular in a diverse range of applications, especially in BCI applications for extracting sensorimotor rhythms. Given the EEG data of two classes (conditions), CSP computes spatial filters that maximize the ratio of the variance of the data of one class to the variance of the other [11]. The spatial filters can be determined by solving the following optimization problem:

$$\mathbf{W}^* = \arg\max_{\mathbf{W}} \{ \frac{\mathbf{W}^T \mathbf{\Sigma}_1 \mathbf{W}}{\mathbf{W}^T \mathbf{\Sigma}_2 \mathbf{W}} \} \tag{1}$$

where $\mathbf{\Sigma}_1$ and $\mathbf{\Sigma}_2$ are covariance matrices from class 1 and 2, respectively. First and last columns of transform matrix $\mathbf{W}^* \in \mathbb{R}^{d \times d}$ contain maximum variances of classes 1 and 2, and can be written as $\mathbf{W}_r = [\mathbf{w}_1 \ \mathbf{w}_d]$. The filtered signal matrix can be expressed as:

$$\tilde{\mathbf{E}}_i = {\mathbf{W}_r}^T \mathbf{E}_i \tag{2}$$

Finally, the feature vector is calculated by

$$\mathbf{x}_i = \text{mean}\left(|\tilde{\mathbf{E}}_i| \right) \tag{3}$$

where $\mathbf{x}_i$ is the feature vector for the i-th trial and $|.|$ is the element-wise absolute value of the matrix.

By assuming that the feature vectors follow a Gaussian distribution and are independent and identically distributed (i.i.d), $\mathbf{x}_i \sim \mathcal{N}(\boldsymbol{\mu}, \mathbf{\Sigma})$, likelihood can be expressed by the Gaussian probability density function. To calculate the covariance of each class, shrinkage and regularization techniques that were proposed for the regularized discriminant analysis (RDA) classifier [12] are recruited. The covariance of each class c is determined as:

$$\hat{\mathbf{\Sigma}}_c(\lambda, \gamma) = (1-\gamma)\hat{\mathbf{\Sigma}}_c(\lambda) + \frac{\gamma}{p} \text{ trace} \left[\hat{\mathbf{\Sigma}}_c(\lambda) \right] \mathbf{I}_p \tag{4}$$

where $\lambda, \gamma \in [0, 1]$ are shrinkage and regularization parameters, respectively. $\mathbf{I}_p$ is a $p \times p$ identity matrix, p is the dimension of feature vectors and $c \in \{0, 1\}$. $\hat{\mathbf{\Sigma}}_c(\lambda)$ is the covariance of class c after passing through the shrinkage process in (5).

$$\hat{\mathbf{\Sigma}}_c(\lambda) = \frac{(1-\lambda) N_c \mathbf{\Sigma}_c + \lambda \sum_{c=0}^{1} N_c \mathbf{\Sigma}_c}{(1-\lambda) N_c + \lambda \sum_{c=0}^{1} N_c} \tag{5}$$

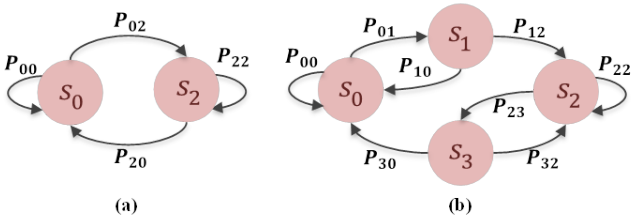

Fig. 3. The Markov chain with four states that represents the transition between different experiment conditions.

N_c is the number of observations in each class. The parameters λ and γ are optimized during calibration session using k-fold cross-validation to maximize the area under the curve (AUC). To estimate the parameters of each class, a set of supervised calibration sessions before starting the online session.

D. Inference Component

The inference component includes a probabilistic model using the concept of Markov chains to synchronize the mirror therapy and robotic training. For the presented experiment procedure, the inter-state transitions between states can be defined by either of the two graphs shown in Fig. 3. In Fig. 3(a), the graph only includes states $\mathbf{s}_0$ and $\mathbf{s}_2$ and the robot status is controlled by the EEG evidence, regardless of the current robot status. The graph in Fig. 3(b), however, includes all states of the experiment and controls the robot based on the EEG evidence and the current robot status. Due to the property of the Markov chain (with order one), the states probability distribution after n trials, $\mathbf{q}_n$ can be expressed as:

$$\mathbf{q}_n = \mathbf{q}_0 \mathbf{P}^n \tag{6}$$

where $\mathbf{P}$ is the transition matrix and $\mathbf{q}_0$ is the initial distribution, which is a row vector. Since the BCI component classification is not always correct, there is an estimation error for state $\mathbf{s}_k$ with probability $P(e_k)$. In graph 1, any classification error, i.e. false positives (FP) in $\mathbf{s}_0$ or false negatives (FN) in $\mathbf{s}_2$ can change the robot status. In fact the robotic training will be affected by the classification errors, which can be inconvenient for patients. In graph 2, however, the robot status can be changed only in $\mathbf{s}_1$ and $\mathbf{s}_3$. It is shown that in the second graph (Fig. 3(b)) the FP and FN errors in $\mathbf{s}_1$ and $\mathbf{s}_3$ are less than graph 1, which means $P(e_3^{g_2}) \leq P(e_0^{g_1})$, $P(e_1^{g_2}) \leq P(e_2^{g_1})$ (see Appendix). Therefore, the graph in Fig. 3(b) is selected for the probabilistic inference.

At each trial, according to the observed EEG evidence $\mathbf{x}_i$ and the last decision $\mathbf{d}_{i-1}$, the inference component makes a decision for the upcoming trial $\mathbf{d}_i$ and updates the experiment state. Each state is defined as $\mathbf{s}_i = [b_i \ r_i]$, where $b_i \in \{0, 1\}$ represents the label of brain activities, i.e. 1 for target class (brain activities due to the mirror therapy) and 0 for non-target class, and $r_i \in \{0, 1\}$ represents the robot status, i.e. 0 when it is off and 1 when it is on. The brain activities label and robot status of each state are equivalent

to the experiment states, such that $\mathbf{s}_0 = [0\ 0]$, $\mathbf{s}_1 = [1\ 0]$, $\mathbf{s}_2 = [1\ 1]$, and $\mathbf{s}_3 = [0\ 1]$. To progress the therapy procedure, the model is used transition probability P^i_{kl} between states k and l, at trial i-th, where $k, l \in [0, 3]$. Using MAP inference, the transition probability P^i_{kl} is determined as:

$$P^i_{kl} = P(\mathbf{d}_i = \mathbf{s}_l | \mathbf{x}_i, \mathbf{d}_{i-1} = \mathbf{s}_k) \tag{7}$$

where $\mathbf{d}_i \in \{\mathbf{s}_0, \mathbf{s}_1, \mathbf{s}_2, \mathbf{s}_3\}$ and

$$\begin{aligned} P(\mathbf{d}_i = \mathbf{s}_l | \mathbf{x}_i, \mathbf{d}_{i-1} = \mathbf{s}_k) \propto \\ P(\mathbf{x}_i | \mathbf{d}_i = \mathbf{s}_l) P(\mathbf{d}_i = \mathbf{s}_l | \mathbf{d}_{i-1} = \mathbf{s}_k) \end{aligned} \tag{8}$$

where $P(\mathbf{x}_i|\mathbf{d}_i = \mathbf{s}_l)$ is the likelihood that is given by the BCI component. Here, it is assumed that $P(\mathbf{x}_i|\mathbf{d}_i = \mathbf{s}_0)$ and $P(\mathbf{x}_i|\mathbf{d}_i = \mathbf{s}_3)$ come from the same distribution. The same assumption exists for $\mathbf{d}_i = \mathbf{s}_1, \mathbf{s}_2$.

III. Results

Five healthy participants (two males), 20-30 years old were recruited to assess the performance of the proposed system. The experiment protocol was approved by the research ethics committee of Northeastern University. No subject had any known neurological disorders. All participants were right-handed and they were asked to move their dominant side (right) ankle as the NAFA. Non-dominant side (left) ankle was assumed as the AFA and was moved by the robot. EEG electrodes were located on the right hemisphere (C2, C4, C6, and CP4) to represent the brain activities of the non-dominant side (due to contralateralization in the human brain). All subjects performed the calibration session. Optimal parameters for target (brain activities due to the mirror image) and non-target classes were learned using the calibration data. The calibration sessions consisted of 240 trials in total. The order of the states were randomized to avoid learning effect during the calibration. The calibration session proceed with a short break (10 minutes) followed by the online session. All subjects started the online session from $\mathbf{s}_0$ and after a few trials (between 3 to 6 trials), they were asked to look at the mirror and imagine the movement of the dominant side limb as the movement of the non-dominant side limb. After a few trails, depending on the observed EEG evidences in the inference component, the robot was turned on to move the non-dominant side ankle ($\mathbf{s}_2$). The online session was ended when the participants stopped looking at the mirror and imagining the left ankle movement. The online sessions included 30 trials on average.

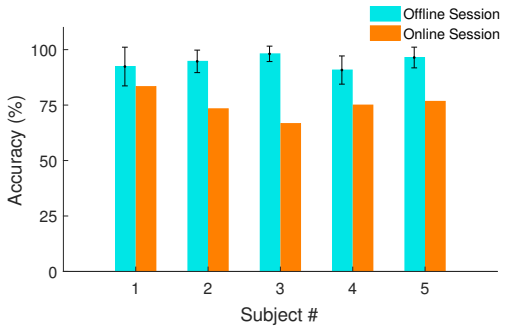

Fig. 4. Performance of the system in offline and online sessions. The error bars present the standard deviation of accuracy across 10-fold cross validation for offline session.

Fig. 4 shows the results of the proposed system performance in offline (calibration) and online sessions for all participants. The accuracy results obtained by the classes trained with offline session EEG data using 10-fold cross validation. During the offline session, participants performed the task at each state separately, without any transition. During the online session, however the participants were performing all tasks consecutively by transiting from one state to another one. The average AUC of the classifier for offline session is 97.5 ± 1.52. Fig. 5 illustrates the normalized confusion matrix that visualized the average performance of the system in the online session. As shown, the system can effectively distinct states $\mathbf{s}_0$, $\mathbf{s}_1$, and $\mathbf{s}_3$. Minimum accuracy belongs to state $\mathbf{s}_2$ that sometimes is mislabeled as $\mathbf{s}_3$.

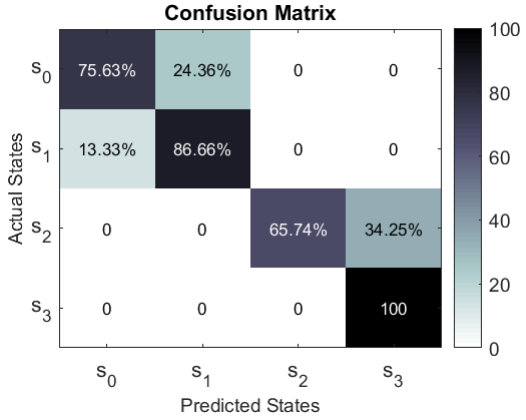

Fig. 5. The normalized average confusion matrix across subjects for online session.

IV. Conclusion and Future Work

An EEG-guided robotic mirror therapy system has been introduced for lower limb rehabilitation. To synchronize the robotic training with the mirror therapy based on the user intention, an experimental paradigm including four states has been suggested. By benefiting from the BCI system, the sensorimotor cortex activities were captured and analyzed to extract EEG evidence. At each state of the experiment, the probabilistic inference has been modeled by a finite-state Markov chain that was defined based on the experiment states. A preliminary experiment was conducted with five healthy subjects including offline and online sessions to validate the feasibility of the system. The preliminary results show high accuracy for both offline and online sessions.

In future work, we aim to assess the therapeutic functionality of the system in lower limb rehabilitation. Moreover, by quantifying a functional recovery in the framework of our therapy method, the chain graph structure can be optimized to maximize the therapeutic objective.

V. APPENDIX

In this section we compare the probability of classification error for both graphs in Fig. 3 and present that the probability of misclassification in each state of graph 2 (Fig. 3(b)) is less than graph 1 (Fig. 3(a)). Let $\mathbf{P}_{g_1}$ and $\mathbf{P}_{g_2}$ be the transition matrices for graph 1 and 2, which are defined as:

$$\mathbf{P}_{g_1} = \begin{bmatrix} 1-\alpha & \alpha \\ \beta & 1-\beta \end{bmatrix}, \ \mathbf{P}_{g_2} = \begin{bmatrix} 1-\alpha & \alpha & 0 & 0 \\ 1-\alpha & 0 & \alpha & 0 \\ 0 & 0 & 1-\beta & \beta \\ \beta & 0 & 1-\beta & 0 \end{bmatrix} \tag{9}$$

where for the same robot status (on/off), it is assumed the probabilities of EEG evidence are the same, which for Fig. 3(b) means $P_{01} = P_{12} = \alpha$ and $P_{23} = P_{30} = \beta$. The confusion matrix of the classifier for each graph is defined as:

$$\mathbf{C}_{g_1} = \begin{bmatrix} N_{TN} & N_{FP} \\ N_{FN} & N_{TP} \end{bmatrix},$$
$$\mathbf{C}_{g_2} = \begin{bmatrix} N_{TN_1} & N_{FP_1} & 0 & 0 \\ N_{FN_1} & N_{TP_1} & 0 & 0 \\ 0 & 0 & N_{TP_2} & N_{FN_2} \\ 0 & 0 & N_{FP_2} & N_{TN_2} \end{bmatrix} \tag{10}$$

where for both graphs, the total number of true positives (TP) is $N_{TP} = N_{TP_1} + N_{TP_2}$, the total number of true negatives (TN) is $N_{TN} = N_{TN_1} + N_{TN_2}$, the total number of false positives (FP) is $N_{FP} = N_{FP_1} + N_{FP_2}$, and the total number of false negatives (FN) is $N_{FN} = N_{FN_1} + N_{FN_2}$. The normalized confusion matrix $\tilde{\mathbf{C}}$ is computed as:

$$\tilde{\mathbf{C}}_{g_1} = \begin{bmatrix} P_{TN} & 1-P_{TN} \\ 1-P_{TP} & P_{TP} \end{bmatrix},$$
$$\tilde{\mathbf{C}}_{g_2} = \begin{bmatrix} P_{TN_1} & 1-P_{TN_1} & 0 & 0 \\ 1-P_{TP_1} & P_{TP_1} & 0 & 0 \\ 0 & 0 & P_{TP_2} & 1-P_{TP_2} \\ 0 & 0 & 1-P_{TN_2} & P_{TN_2} \end{bmatrix} \tag{11}$$

Using (6), the probability distribution for the i-th trial is defined as $\mathbf{q}_i = \mathbf{q}_{i-1}\mathbf{P}$. To identify which graph leads to lower classification error for each state, $P(e_k)$ is computed for both graphs as follows:

$$\begin{aligned} P(e_k^{g_1}) &= \begin{cases} P(\mathbf{x}_i \in R_2,\ \mathbf{d}_i = \mathbf{s}_0),\ k=0 \\ P(\mathbf{x}_i \in R_1,\ \mathbf{d}_i = \mathbf{s}_2),\ k=2 \end{cases} \\ P(e_k^{g_2}) &= \begin{cases} P(\mathbf{x}_i \in R_2,\ \mathbf{d}_i = \mathbf{s}_0),\ k=0 \\ P(\mathbf{x}_i \in R_1,\ \mathbf{d}_i = \mathbf{s}_1),\ k=1 \\ P(\mathbf{x}_i \in R_1,\ \mathbf{d}_i = \mathbf{s}_2),\ k=2 \\ P(\mathbf{x}_i \in R_2,\ \mathbf{d}_i = \mathbf{s}_3),\ k=3 \end{cases} \end{aligned} \tag{12}$$

where R_1 and R_2 present the distributions of class 1 and 2 respectively, and $P(\mathbf{x}_i \in R_2,\ \mathbf{d}_i = \mathbf{s}_0)$ is the probability of predicting the observation $\mathbf{x}_i$ falls in R_2, however the true label is 0 that belongs to $\mathbf{s}_0$. This probability is defined as:

$$P(\mathbf{x}_i \in R_2,\ \mathbf{d}_i = \mathbf{s}_0) = P(\mathbf{x}_i \in R_2 | \mathbf{d}_i = \mathbf{s}_0) P(\mathbf{d}_i = \mathbf{s}_0) \tag{13}$$

where $P(\mathbf{x}_i \in R_2 | \mathbf{d}_i = \mathbf{s}_0) = 1 - P_{TN}$ and $P(\mathbf{x}_i \in R_1 | \mathbf{d}_i = \mathbf{s}_2) = 1 - P_{TP}$. For graph 1, by assuming $\mathbf{q}_{i-1} = [q \ \ 1-q]$, the misclassification errors are calculated as:

$$\begin{aligned} P(e_0^{g_1}) &= [q(1-\alpha) + (1-q)\beta]\,(1-P_{TN}) \\ P(e_2^{g_1}) &= [q\alpha + (1-q)(1-\beta)]\,(1-P_{TP}) \end{aligned} \tag{14}$$

For graph 2, by assuming $\mathbf{q}_{i-1} = [q \ \ 0 \ \ 1-q \ \ 0]$, the error for each state is calculated as:

$$\begin{aligned} P(e_0^{g_2}) &= q(1-\alpha)(1-P_{TN_1}) \\ P(e_1^{g_2}) &= q\alpha(1-P_{TP_1}), \\ P(e_2^{g_2}) &= (1-q)(1-\beta)(1-P_{TP_2}), \\ P(e_3^{g_2}) &= (1-q)\beta(1-P_{TN_2}), \end{aligned} \tag{15}$$

Since the classifier accuracy for each class is the same for both graphs, $P(e_0^{g_1}) = P(e_0^{g_2}) + P(e_3^{g_2})$, which means $P(e_3^{g_2}) \leq P(e_0^{g_1})$. Equivalently, $P(e_2^{g_1}) = P(e_1^{g_2}) + P(e_2^{g_2})$, which means $P(e_1^{g_2}) \leq P(e_2^{g_1})$. This shows that the probability of misclassification in $\mathbf{s}_1$ and $\mathbf{s}_3$ that control the robotic training in graph 2 is less than $\mathbf{s}_0$ and $\mathbf{s}_2$ in graph 1.

REFERENCES

[1] M. A. Dimyan and L. G. Cohen, "Neuroplasticity in the context of motor rehabilitation after stroke," *Nature Reviews Neurology*, vol. 7, no. 2, pp. 76–85, 2011.

[2] J.-M. Belda-Lois, S. Mena-del Horno, I. Bermejo-Bosch, J. C. Moreno, J. L. Pons, D. Farina, M. Iosa, M. Molinari, F. Tamburella, A. Ramos *et al.*, "Rehabilitation of gait after stroke: a review towards a top-down approach," *Journal of neuroengineering and rehabilitation*, vol. 8, no. 1, p. 66, 2011.

[3] P. W. Duncan, K. J. Sullivan, A. L. Behrman, S. P. Azen, S. S. Wu, S. E. Nadeau, B. H. Dobkin, D. K. Rose, J. K. Tilson, S. Cen *et al.*, "Body-weight-supported treadmill rehabilitation after stroke," *New England Journal of Medicine*, vol. 364, no. 21, pp. 2026–2036, 2011.

[4] M. E. Michielsen, R. W. Selles, J. N. van der Geest, M. Eckhardt, G. Yavuzer, H. J. Stam, M. Smits, G. M. Ribbers, and J. B. Bussmann, "Motor recovery and cortical reorganization after mirror therapy in chronic stroke patients: a phase ii randomized controlled trial," *Neurorehabilitation and Neural Repair*, vol. 25, no. 3, pp. 223–233, 2011.

[5] S. Saleh, S. V. Adamovich, and E. Tunik, "Mirrored feedback in chronic stroke: recruitment and effective connectivity of ipsilesional sensorimotor networks," *Neurorehabilitation and neural repair*, vol. 28, no. 4, pp. 344–354, 2014.

[6] J. J. Daly and J. R. Wolpaw, "Brain-computer interfaces in neurological rehabilitation," *The Lancet Neurology*, vol. 7, no. 11, pp. 1032–1043, 2008.

[7] K. K. Ang and C. Guan, "Brain-computer interface in stroke rehabilitation," *Journal of Computing Science and Engineering*, vol. 7, no. 2, pp. 139–146, 2013.

[8] A. H. Do, P. T. Wang, C. E. King, S. N. Chun, and Z. Nenadic, "Brain-computer interface controlled robotic gait orthosis," *Journal of neuroengineering and rehabilitation*, vol. 10, no. 1, p. 111, 2013.

[9] W.-P. Teo and E. Chew, "Is motor-imagery brain-computer interface feasible in stroke rehabilitation?" *PM&R*, vol. 6, no. 8, pp. 723–728, 2014.

[10] A. B. Farjadian, S. Suri, A. Bugliari, P. Douçot, N. Lavins, A. Mazzotta, J. P. Valenzuela, P. Murphy, Q. Kong, M. K. Holden *et al.*, "virabt: Virtually interfaced robotic ankle and balance trainer," in *2014 IEEE International Conference on Robotics and Automation (ICRA)*. IEEE, 2014, pp. 228–233.

[11] Y. Wang, S. Gao, and X. Gao, "Common spatial pattern method for channel selelction in motor imagery based brain-computer interface," in *Engineering in Medicine and Biology Society, 2005. IEEE-EMBS 2005. 27th Annual International Conference of the*. IEEE, 2006, pp. 5392–5395.

[12] J. H. Friedman, "Regularized discriminant analysis," *Journal of the American statistical association*, vol. 84, no. 405, pp. 165–175, 1989.